Essential Readings in Light Metals: Aluminum Reduction Technology.
Edited by Geoff Bearne, Marc Dupuis and Gary Tarcy.

Light Metals — From *Light Metals 1994*, Ulrich Mannweiler, Editor

PRODUCTION OF ALUMINUM WITH LOW TEMPERATURE FLUORIDE MELTS

Theodore R. Beck
Electrochemical Technology Corp.
1601 Dexter Ave. North
Seattle, WA 98109, USA

ABSTRACT

Low cell operating temperature is desirable to minimize corrosion and promote long life of dimensionally-stable anodes and cathodes. Eutectic NaF-AlF_3 melts, with and without added LiF-AlF_3 and KF-AlF_3, have been evaluated in 1 - 40 A laboratory cells at about 750°C over a period of four years with various values of the operating parameters. Particles of Al_2O_3, suspended in the bath by O_2 bubble evolution, dissolve in the anode boundary layer and prevent anode effect to greater than 2 A/cm^2. Operation with multiple, vertical, monopolar anodes and cathodes at 0.5 A/cm^2 each side promises a 20-fold decrease in cell volume compared to conventional H-H cells, with an accompanying decrease in capital cost. Projected specific energy consumption is about 11 kwh/kg.

INTRODUCTION

The aluminum industry has long been interested in dimensionally-stable cathodes (1) and non-consumable anodes (2). A satisfactory non-consumable anode would have numerous advantages including elimination of the carbon anode plant, of anode changes, and of potential CF_4 and CO_2 environmental problems, as the overall reaction would be

$$Al_2O_3 \rightarrow 2Al + 3/2\ O_2 \qquad (1)$$

Combination of dimensionally-stable anodes and cathodes would permit lower-cost, more-efficient cell designs. Most of the prior work reported with dimensionally-stable anodes and cathodes was with conventional cryolyte electrolyte at temperatures of about 950°C and results have been disappointing due to corrosion and fracture.

The thrust of the present work is to use lower-melting fluoride electrolytes which can be operated at about 750°C to minimize corrosion and fracture of electrodes. A problem to be overcome at the lower temperature is lower solubility of alumina with resultant anode effects. It was shown earlier that feeding alumina to the anode-electrolyte interface in a composite Al_2O_3/carbon anode solved this problem (3). In the present work it is shown that Al_2O_3 particles may be fed in suspension in the electrolyte to the anode-electrolyte interface to avoid anode effect and give near saturation of Al_2O_3 at the interface. Near saturation of Al_2O_3 has been shown to be beneficial for cermet anode operation under conventional Hall-Heroult cell conditions (4) and the present work indicates it is beneficial at lower temperatures.

Much of the present laboratory work was carried out with copper anodes in seven-hour tests. Copper was perfectly satisfactory for tests of electrolyte composition and characterizing the performance of suspended Al_2O_3 particles, although the oxidation rate of copper is too high for commercial cell operation. During the course of this work a new anode was developed which will be described in a later paper.

LABORATORY CELLS

The design of the cell used for most of the laboratory tests is shown in Fig. 1. An alumina crucible was placed inside a 304 stainless steel can which contained the bath in the event of a crucible fracture and which had a lifting tab to remove the cell from the furnace. The furnace was built of firebrick with a bottom heater and clamshell side heaters. Anodes in the early runs were copper disks about 5 cm in diameter. A heavy copper wire was peened into a hole at the edge to make electrical connection. An alumina tube insulated the copper wire in the bath. In later runs the new proprietary anode was used. In some runs an additional annular copper anode, 5 cm in diameter and extending up to the bath surface, permitted higher cell currents up to 50 amperes. In this paper, electrolyte is defined as the mixture of fluorides, and bath is electrolyte plus suspended Al_2O_3 particles and entrained oxygen gas bubbles.

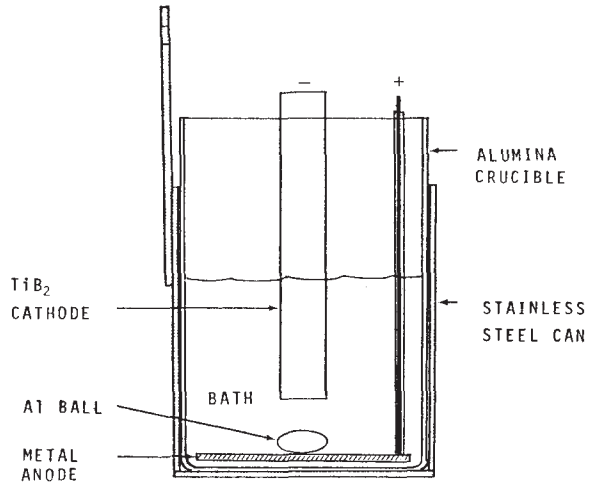

Fig. 1 Alumina crucible cell

The cathode was a 2.3 cm diameter, 10 cm long TiB_2 rod. Electrical connection was made to a flattened stainless steel tube at the top with a hose clamp. In many of the runs the hose clamp was coated with an alumina cement to minimize airburn of the TiB_2. Corrosion of the TiB_2 immersed in bath was too small to measure after hundreds of hours of runs. Aluminum produced on the cathode dripped off and formed a ball which was levitated by oxygen bubbles produced on the anode. It may be counter-intuitive to have the aluminum near the anode, but results presented here show that the system works. A side benefit of the saturated alumina electrolyte is that alumina thermocouple tubes can be used for continuous temperature measurement.

A second cell used in anode effect tests was a graphite crucible with an alumina liner which restricted cathodic current to the bottom of the crucible. Cathode connection was made through a stainless steel can. The top-entering anode was graphite or, in later runs, the new proprietary anode.

A third cell to operate at 300 amperes was built, but available funding and time allowed only a few-hour test run. The proprietary anode was used with TiB_2 cathodes. The vertical electrode plates were about 14 cm tall and the anode-cathode spacing was about 1.3 cm.

ELECTROLYTE

The electrolytes used were the eutectic NaF-AlF_3 and eutectic NaF-KF-LiF-AlF_3 mixtures. Very precise control of composition is required to avoid either precipitation of cryolite at the cathode (5) or AlF_3 at the anode (6). The binary phase diagram (7) in Fig. 2 shows the concentration differences for the precipitations of cryolite and AlF_3. The ΔC_2 for precipitation of AlF_3 at the anode is smaller than the ΔC_1 for cryolite precipitation at the same current density mainly because the mass transfer coefficient is larger at the gas-evolving anode. At the eutectic composition of 44±1 mol% AlF_3 the cell could be operated satisfactorily at 0.5 A/cm^2. Addition of KF-AlF_3 and LiF-AlF_3 eutectics gave a wider mol% AlF_3 composition range because of the lower eutectic temperatures (8).

The electroytes were prepared from reagent-grade NaF, KF, and LiF of >99% purity and smelter-grade AlF_3 containing about 9% Al_2O_3. At the eutectic 44 mol% AlF_3 the bath compositions tended to remain nearly constant during 7-hour runs because the small amount of vaporizing species, $NaAlF_4$ (7), with 50 mol% AlF_3, is close to the eutectic composition.

Throughout this paper bath compositions are given in mol% AlF_3. To convert to the equivalent weight ratio of NaF to AlF_3 in the binary bath, used in the industry, the following formula is used:

$$wt\ ratio,\ NaF{:}AlF_3 = 0.50\ (\frac{100}{y} - 1) \qquad (2)$$

in which y = mol% AlF_3. Thus y = 44 mol% gives a weight ratio of 0.64.

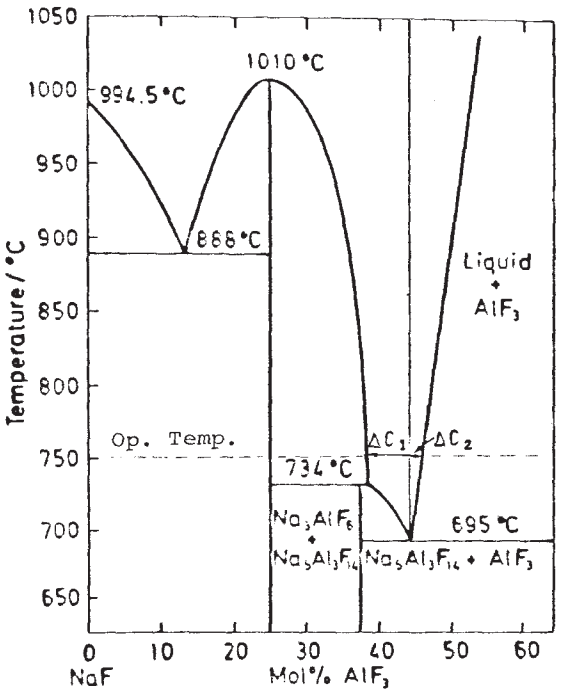

Fig. 2 Phase diagram of the system NaF-AlF_3; from Grjotheim, et al., (7)

Estimated properties of the eutectic electrolyte at 750°C compared to cryolite at 980°C are given in Table 1 based on interpolations and extrapolations of data in Grjotheim, et al. (7). The big differences are the order of magnitude lower Al_2O_3 solubility and diffusivity. The electrical conductivity is also decreased. The lower Al_2O_3 solubililty and diffusivity are overcome by the suspended particulate Al_2O_3. The lower electrical conductivity is overcome by a smaller anode-cathode spacing and a lower current density than in a conventional Hall-Heroult cell.

Table 1
Estimated Properties of Eutectic Electrolyte at 750°C Compared to Cryolite at 980°C

	1.5 Ratio Cryolite 980°C	Eutectic Bath 750°C
Melting points, °C	1009*	695
Al_2O_3 solubility, wt%	10	~1
Density, g/cm^3(w/o Al_2O_3)	2.1	2.0
Viscosity, c.p.	2.6	4.
Conductivity, S/cm	2.8	1.3
Al_2O_3 diffusion coef., cm^2/s	~2 x 10^{-5}	~0.3 x 10^{-5}
Al density	2.29	2.36
ρ Al-ρ elec. (w/o Al_2O_3)	0.2	0.4

* Melting point of cryolyte is lowered by CaF and by dissolved Al_2O_3

SUSPENSION OF ALUMINA PARTICLES

Settling velocities of alumina particles in the electrolyte at 750°C can be calculated using Stokes law (9) (See Table of Nomenclature)

$$u_t = \frac{2(\rho_p - \rho_e) g\, r^2}{9\ \mu} \qquad (3)$$

The parameter values used are ρ_p = 4 g/cm^3, ρ_e = 2 g/cm^2, g = 980 cm/s^2, and μ = 0.04 g/s·cm (estimated in Table 1). Velocities are plotted versus particle diameter in Fig. 3 for a diameter range from 1 to 50 μm.

Velocities of oxygen bubbles are similarly calculated for ρ_p = o, which gives negative or upward velocities on the same line as for the alumina particles. The observed bubble diameters were 1 to 2 mm diameter from copper anodes. Oxygen bubbles from cermet anodes were reported to be in the diameter range, 0.1 to 0.5 mm (4). The 0.1 to 2 mm range is plotted in Fig. 3. Velocities of aluminum droplets, for which the density difference based on slurry was assumed to be 0.2 g/cm^3, were calculated for 1 to 10 mm diameters and also plotted in Fig. 3. The use of wetted TiB_2 cathodes avoids formation of smaller aluminum droplets.

Bath circulation velocity was calculated by equating the buoyancy force of the oxygen bubbles to the friction, expansion and contraction forces as the bath circulates, by the method of MacMullin (10). A commercial cell with vertical electrode heights of 30 cm, an anode-cathode spacing of 1 cm, and a current density of 0.5 A/cm^2 on each side of each electrode gave a calculated velocity of about 50 cm/s. A laboratory cell with electrode height of 2.5 cm gave a calculated velocity of 15 cm/s. By these calculations, Al_2O_3 particles should remain suspended and O_2 bubbles escape and aluminum droplets sink to the bottom.

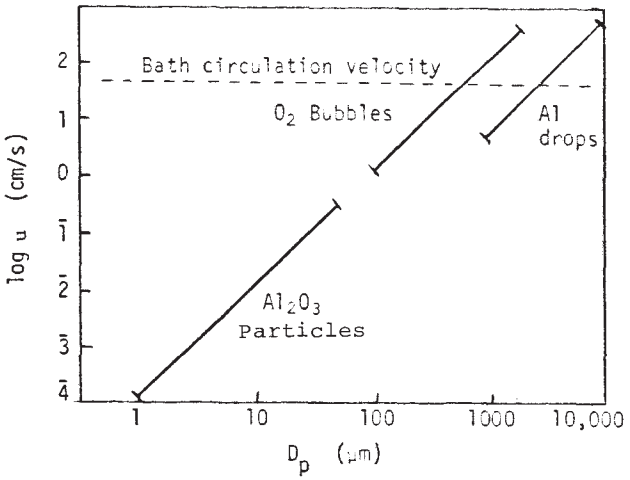

Fig. 3 Settling velocities in bath as a function of particle diameter

Observations with the laboratory cells, Fig. 1, showed that O_2 bubbles escape, aluminum droplets coalesce and sink to the bottom, and Al_2O_3 particles remain suspended when using a bottom anode. The suspended Al_2O_3 particles cause the electrolyte to be opaque and have a milky appearance. With only an annular vertical anode and no bottom anode the Al_2O_3 particles settled out in spite of the circulation velocity being greater than the settling velocity. Settling of particles and formation of muck in this case can be attributed to deadspots in the cell or to regions of slow, horizontal velocity where the settling time is less than the horizontal transit time. Once a particle is deposited on the bottom without a bottom anode, it becomes part of a "new bottom" of muck that can continue to grow. Muck with, for example, 25% by volume of particles is viscous and has a density of about 2.6. An auxilliary bottom anode is a necessary condition.

MASS TRANSPORT TO ANODE

Three main mechanisms for transport of alumina to the anode surface are considered:

- Nerstian diffusion of dissolved Al_2O_3;
- Convection of bath by gas bubble disengagement;
- Diffusion from dissolving Al_2O_3 particles within the Nernst layer.

The limiting current density for the first mechanism appears to be too low. A combination of the second two mechanisms appears to be the case based on experimental results obtained. For diffusion of the neutral species, Al_2O_3, the transference number is unity and Fick's first law applies, uncorrected, for the conceptual stagnant Nernst diffusion layer.

The diffusion from dissolving Al_2O_3 particles in the Nernst layer is depicted in Fig. 4. The derivation is valid for the condition that the particle diameter is smaller than the Nernst diffusion layer thickness, δ_N, without particles. Al_2O_3 particles of radius r in the bath dissolve in the unsaturated region close to the anode. The Al_2O_3 is considered to dissolve from the surface of a particle and diffuse away radially near the particle. The dissolved Al_2O_3 transported by normal flux, j_x, is discharged on the anode surface.

$$Al_2O_3 \rightarrow 2\ Al^{3+} + 3/2\ O_2 + 6\ e^- \qquad (4)$$

The excess Al^{3+} ions after leaving the anode region by diffusion and migration are carried by convection in the bath to the region of the cathode where they are discharged. Formation and disengaging of oxygen bubbles at the anode continually brings fresh particles in slurry to the anode surface region.

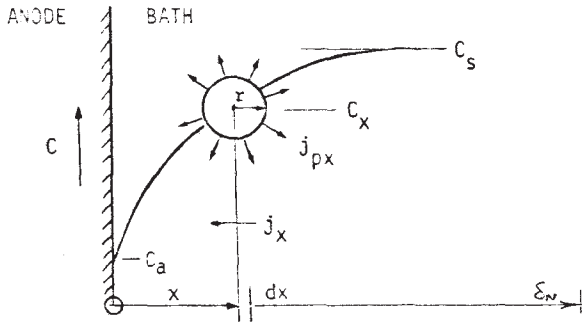

Fig. 4 Diffusion flux in boundary layer

The derivation will be presented elsewhere, but the resulting limiting current density is

$$i_L = \frac{6\ F\ D\ C_s}{r}\sqrt{\frac{3\ W \rho_b}{100\ \rho_p}} \qquad (5)$$

or

$$i_L = a\ W^{1/2} \qquad (6)$$

in which a is a constant for a given temperature and particle size. For 0.5 μm radius particles and parameter values in Table 1, the value of a is 0.89 $A/cm^2 \cdot \%^{1/2}$. Application of Faraday's law and the condition that the net suspended Al_2O_3 is the total minus the solubility, gives a relation of i_L to time

$$i_L = a\sqrt{W_t\ (initial) - W_s - 0.030\ \epsilon\ t} \qquad (7)$$

for a current of 20 amperes and an electrolyte volume of 320 cm^3 for the anode effect test cell. In the experiments, W_t(initial) = 4.5 percent from the smelter grade AlF_3 and W_s is estimated to be about 1 wt%. The operating current density at 20 A was 0.5 A/cm^2, and periodically the current was ramped up to anode effect.

Data on current density at anode effect for a run with A-152 SG alumina are in Fig. 5. The A-152 SG with mean particle diameter of about 1 μm is the ground alumina that was used in nearly all of the runs. The run started with alumina from the AlF_3 and additional A-152 SG was added when the original was nearly depleted, and a second set of data was obtained. Equation 7 was fitted to two points and values of a and ε were determined as shown in Table 2. The equation was plotted through the data points in Fig. 5. Values of a and ε for three other runs are also given in Table 2. Surprisingly, the run with added 10 μm diameter particles showed only a small decrease in the value of a after the addition of Al_2O_3. Equation 5 would predict a 10-fold decrease. Some remaining initial small particles and some disintegration of larger particles may have contributed to this result. There is approximate agreement between the values of current efficiency calculated from Eq. 7 and those measured for whole runs based on aluminum recovered.

Thonstad (11) pointed out that unpublished data from Trondheim show that reduction grade alumina particles break up in cryolite bath saturated with Al_2O_3 at 1000°C. Reduction-grade alumina particles are about 100 μm in diameter and are agglomerations of smaller particles. Long-term tests are planned to determine if the particles break up sufficiently fast in eutectic NaF/AlF_3 at 750°C.

Table 2

Experimental Values of a and ϵ

Alumina	Mean diam μm	a initial	a 2nd	ϵ initial	ϵ 2nd	ϵ for run
A-152	1	1.19	1.23	0.50	0.78	0.29
A-10-325	10	1.64 1.78	- 1.13	0.80* 0.50	- 0.27	0.63
A-3(Gnd)	1	1.55	1.59	0.53	0.43	0.31
A-3(Gnd)	1	1.58	1.20	0.55	0.47	0.53

* current density = 1A/cm²

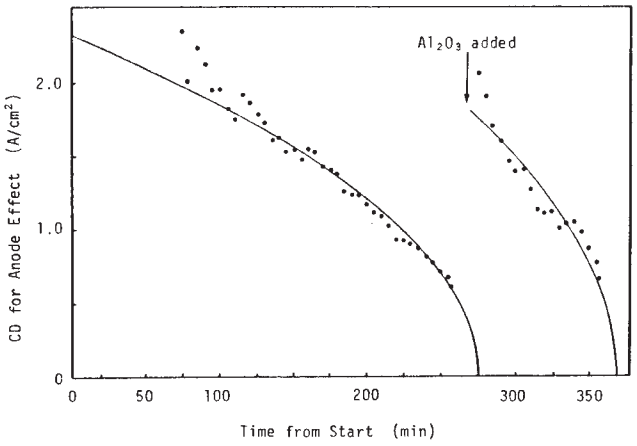

Fig. 5 Test of mass transfer model
• cell data
– equation 7 fit to data

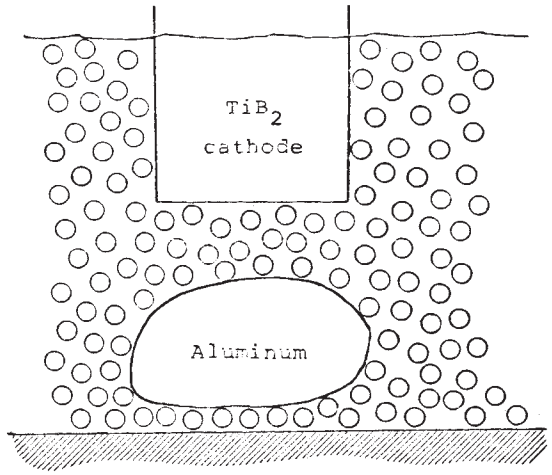

Fig. 6 Aluminum ball on bottom of cell levitated by oxgen bubbles from the anode

CURRENT EFFICIENCY

Current efficiency for a large number of 7-hour runs has averaged about 50% at a current of 12 A. A 50% back reaction of an aluminum ball close to a vigorous-oxygen-bubbling anode as shown in Fig. 6 should not be surprising. The rate of the parasitic back reaction can be empirically described by

$$R_p = k\,A\,\Delta C \qquad (8)$$

in which k is a mass transfer coefficient in cm/s, A is the surface area of the aluminum ball in cm², and ΔC is a concentration driving force for the back reacting species in mol/cm³. Individual values of k and ΔC are undefined yet for this system so the values are lumped. To simplify, it is assumed that the mass transfer coefficient is uniform around the surface of the ball, even though it is probably higher on the underside subject to more vigorous agitation by O_2 bubbles. The rate of the parasitic back reaction can be expressed in terms of an equivalent current for reoxidation of Al to Al^{3+}.

$$I_p = 3\,F\,k\,A\,\Delta C \qquad (9)$$

Current efficiency for the cell is then

$$\epsilon = \frac{I - I_p}{I} \qquad (10)$$

or

$$\epsilon = 1 - 3\,F\,k\,\Delta C\left(\frac{A}{I}\right) \qquad (11)$$

It is assumed that back reaction of aluminum on the TiB_2 cathode is negligible because it is cathodically protected and it is at a 200°C lower temperature than in conventional Hall-Heroult cells. It may be also assumed that kΔC remains approximately constant on scaling up a cell. To obtain increased current efficiency the value of A/I must be kept small. In the test cell (Fig. 1) about a 2 cm diameter ball of aluminum with area of 15 cm² is produced in 7 hours at 12 A and 50% current efficiency. The value of 3FkΔC from equation 11 is then approximately 0.5/(15/12) = 0.4 A/cm². When the ball of aluminum can be kept small in a commercial cell by continuous removal, the predicted current efficiency would be close to 100%

The validity of Eq. 11 was tested by comparing to a representative set of laboratory cell data with a bottom anode and with currents ranging from 6 to 46 amperes at i ≤ 0.5 A/cm². Equation 11 was rearranged to the form

$$\left(\frac{1}{1-\epsilon}\right) = \left(\frac{1}{KA}\right) I \qquad (12)$$

in which K = 3FkΔC. Run data are plotted in Fig. 7. A straight line was drawn through the origin in accordance with Eq. 12, giving a slope (1/KA) = 0.148 A⁻¹. Equation 11 with this value of KA is

$$\epsilon = 1 - \frac{6.76}{I} \qquad (13)$$

Equation 13 for A = 15 cm² is plotted in Fig. 8 with the cell data. The current efficiencies at low currents are above the curve and at high currents below the curve. The reason is probably that the aluminum ball is smaller at low current and larger at high current. Example curves for half the area and for twice the area in Eq. 13 are drawn to illustrate this effect. In runs in which nitrogen gas was used for agitation, the metal ball was broken up into small drops with greater total surface and the current efficiencies were very small or even zero.

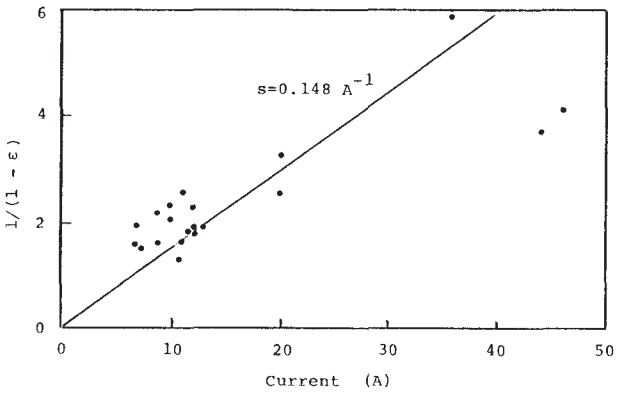

Fig. 7 Plot of cell current efficiency data on coordinates of Eq. 12

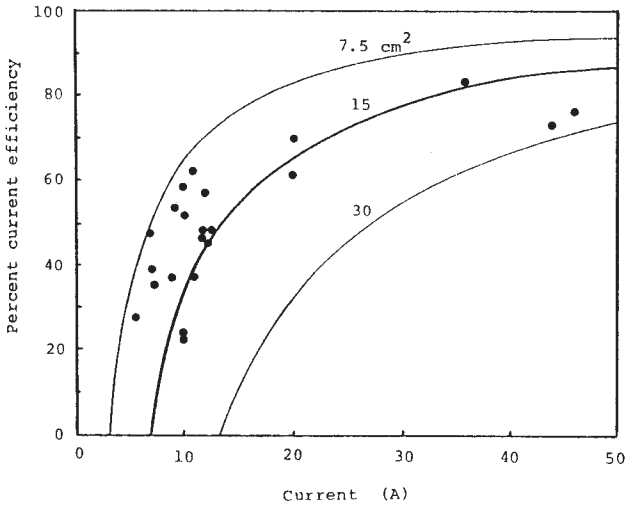

Fig. 8 Plot of cell current efficiency data versus current; lines are Eq. 11 with aluminum ball area as parameter

OTHER CONSIDERATIONS

Bath Density

The bath consists of electrolyte, suspended Al_2O_3 particles and entrained oxygen bubbles. The estimated density of the electrolyte from Table 1 is 2.0 g/cm^3. The calculated density for a bath with 10 wt% Al_2O_3 (density 4.0) is

$$\rho = 1/(0.9/2.0 + 0.1/4.0) = 2.10 \text{ g/cm}^3$$

It was found in the 300 A cell that the O_2 bubbles occupied about 10 volume % by observing the bath height change by turning the current off and on. A 10 vol% of O_2 bubbles would give a density of

$$\rho = (0.9)(2.10) + (0.1)(0) = 1.90 \text{ g/cm}^3$$

Aluminum metal droplets of density 2.36 g/cm^3 should therefore sink to the bottom of the bath, and indeed aluminum metal droplets were never seen at the top of the bath in any laboratory tests.

Without O_2 bubbling from the bottom of the cell the particulate Al_2O_3 can settle out and form muck. The density of muck is variable depending on the concentration of the Al_2O_3 particles. For 50 vol% Al_2O_3 in the muck, the density would be

$$\rho = (0.5)(2.10) + (0.5)(4.0) = 3.0 \text{ g/cm}^3$$

and any aluminum droplets would float on top of the muck. This effect prevents aluminum droplets from contacting directly and reacting with the bottom anode in the event of a loss in current.

Cell Voltage

The total cell voltage is composed of the thermodynamic reversible potential based on the free energy of reaction (1) plus overpotentials at the electrodes and ohmic drops in the bath and electrodes. The free energy of formation of α Al_2O_3 at 1000°K (727°C) is -325.3 kcal/mol (12), giving a thermodynamic potential of 2.35 V for a 6-electron reaction. The anode overpotential at 0.5 A/cm^2 was estimated to be about 0.3 V from polarization curves and cathode overpotential is negligible. The bath ohmic drop is

$$E_b = \frac{i\,\ell}{\kappa} \qquad (14)$$

in which ℓ is the anode-cathode spacing and κ is the effective conductivity of the bath. The conductivity of electrolyte, 1.3 S/cm (Table 1), is corrected for 10 wt% Al_2O_3 particles and 10 vol% O_2 bubbles. The first correction for approximately 5 vol% Al_2O_3 is about 0.92 (13) and the second correction for 10 vol% O_2 is about 0.85 (13). The effective bath conductivity is then (1.3)(0.92)(0.85) = 1.0 S/cm. The bath ohmic drop for a 1.3 cm anode cathode spacing and 0.5 A/cm^2 is then 0.65 V. Electrode voltage drop was estimated to be 0.2 V, giving the 3.5 V measured across the 300 A cell at 0.5 A/cm^2. The enthalpy of formation of Al_2O_3 at 1000°K is -404.5 kcal/mol (12), giving an adiabatic potential of 2.92 V. The difference between this value and the operating potential of about 3.5 V is 0.6 V, which in a self-sustaining large commercial cell would be used to bring the Al_2O_3 reactant up to temperature and make up heat losses. The thermal efficiency of the cell is then about 83%.

Continuous Removal of Aluminum

Aluminum produced must be continuously removed from a commercial cell having a bottom auxilliary anode, to avoid shielding and stopping O_2 evolution which keeps the Al_2O_3 particles from settling. Devices are under development to continuously remove aluminum produced.

PROPOSED COMMERCIAL CELL DESIGN

A proposed commercial cell design and mode of operation are presented here based on the experimental work and patents issued (14-16).

The main departures from existing Hall-Heroult technology are the following:

- An eutectic electrolyte with freezing point below 695°C, either NaF plus AlF_3 or a mixture of NaF/AlF_3, and KF/AlF_3 plus LiF/AlF_3 eutectics operating at about 750°C.
- A 5-10 wt% slurry of Al_2O_3 with particle size less than 10 μm. Reduction grade Al_2O_3 with 100 μm agglomerated particles may break down in the electrolyte to its component 10 μm and less particles.
- Vertical monopolar anodes and vertical, close-spaced, monopolar TiB_2 cathodes.
- A horizontal auxilliary anode on the bottom of the cell which generates O_2, keeping Al_2O_3 from settling and forming muck.
- A device which continuously transports aluminum produced out of the cell.

The main features of the present conceptual cell design (14-16) including the vertical TiB_2 cathodes and non-consumable anodes and bottom auxilliary anode are shown in Fig. 9. A monopolar electrode configuration is preferred to avoid bonding problems of dissimilar anode and cathode materials and to avoid edge corrosion of the cathodes (17). An insulated hood (not shown) is used so the cell operates without frozen ledge or crust. Aluminum deposited on the TiB_2 cathodes flows down their sides and drips off their pointed bottoms along the centerline of the cell. Aluminum balls then roll down the inclined centerline of the cell to a collection point where they agglomerate and are removed continuously. Current is carried into the cell from the

adjacent side-to-side cell by flexible leads from the intercell equalizing bus. Current is carried out from each cathode by a TiB_2 rod protected from airburn by an alumina sleeve. Flexible leads make connection to the next adjacent equalizer bus. Alumina is fed through the hood and is heated by radiation before it hits the bath, avoiding bath freezing. Evolved O_2 is removed through the hood to the collection system. A smaller air flow than for conventional cells can be used because of better seals on the hoods, and no openings are required for anode change or crust breaking as in conventional cells. Bath temperature is measured continuously with a thermocouple in an alumina tube, 45.

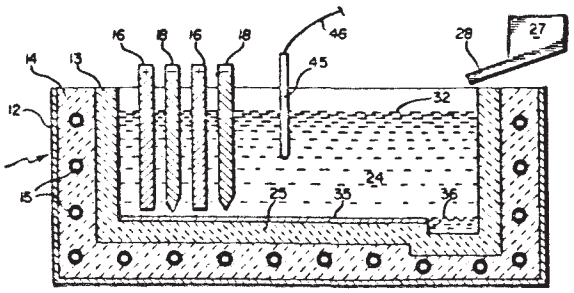

Fig. 9 Conceptual commercial cell design (16)

An isometric drawing showing a comparison of the size of a modern conventional 200 kA Hall-Heroult cell to a 200 kA slurry cell is given in Fig. 10. The conventional cell is about 15 ft wide, 35 ft long, and 3 ft high, plus about 6 ft of superstructure. The slurry cell contains 100 anode/cathode pairs with 2 sq ft per side for a total of 400 sq ft each of anode and cathode, giving a current density of about 0.5 A/cm^2. Anodes are assumed to be 0.4 in. thick, cathodes 0.8 in. thick, and anode-cathode spacing of 0.5 in.

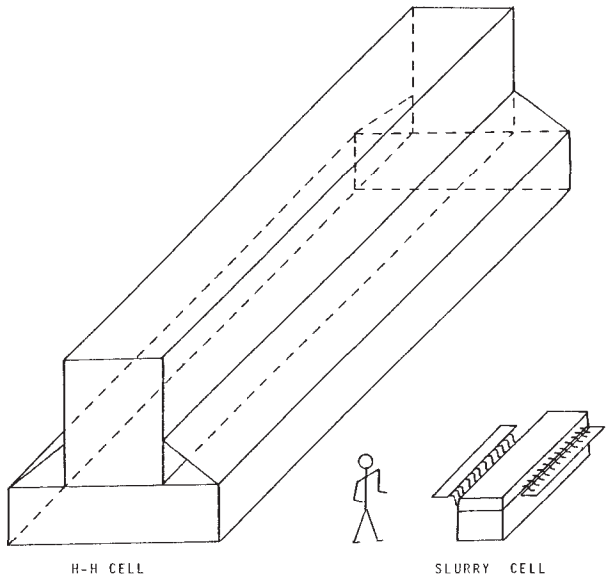

Fig. 10 Isometric comparison of size of conventional Hall-Heroult cell to slurry cell; 200 kA; 6-ft man

The 200 kA slurry cell envisaged in Fig. 9 and 10 fits on the correlation of reactor volume versus throughout developed by Waldron (18) for a wide range of processes shown in Fig. 11. The conventional 200 kA Hall-Heroult cell has more than an order of magnitude larger volume because of the spatial inefficiency of a single horizontal anode and cathode per cell. The filled circles in Fig. 11 were calculated by the author.

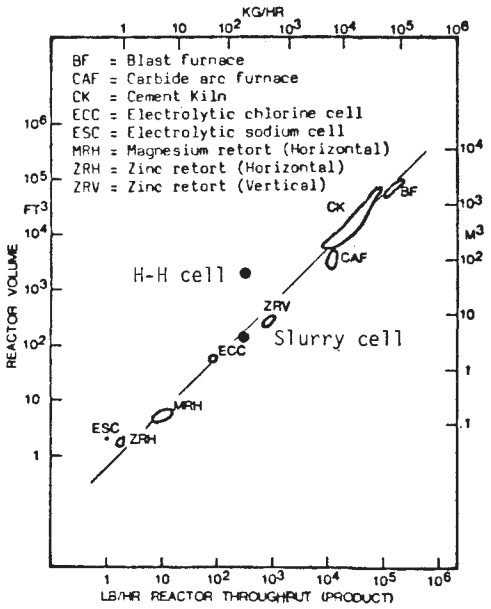

Fig. 11 Comparison of 200 kA Hall-Heroult cell and 200 kA slurry cell to reactor volume/throughput correlation of Waldron (18)

A brief overall comparison of the major tradeoffs for the new non-consumable anode/slurry cell technology to the conventional Hall-Heroult technology is given in Table 3. The tradeoffs and larger advantages favor the new technology.

Size of cells and potrooms are considerably reduced with accompanying decrease in capital cost. Carbon anode manufacturing facilities are also eliminated. Consideration of a distribution of capital in a 200,000 ton/yr prebake plant indicates a possible capital saving of 40% to 50% for a greenfield plant. Retrofit of an existing plant would require new capital, but the payout time is estimated at 2 to 4 years depending on the plant.

Specific energy consumption could be decreased from 13-17 kWh/Kg to about 11 kWh/Kg. A 4 kWh/Kg average saving would give a 8¢/Kg saving for 20 mil/kWh energy. Elimination of carbon anode production and anode change would save another 8¢/Kg. A possible future general tax on CO_2 emissions of $100/ton aluminum (21) or 11¢/Kg would be eliminated by non-consumable anodes. Emission of ozone-depleting perfluorocarbons (PFCs) (20) will be eliminated, thus avoiding possible penalties by EPA.

Frozen bath ledges and crust and muck under the aluminum metal pad, which are difficult to control will be eliminated with the new technology. A new dimension of continuous temperature measurement becomes economically feasible with alumina thermocouple tubes with the new technology. Potroom fume treatment systems can be smaller with new smaller cells without carbon anode changes.

On the negative side, the new technology may require a finer particle size or perhaps more-friable aluimina agglomerate particles. In time the industry could convert to the new alumina grades if necessary and there would be no cost penalty. Bath ratio or AlF_3 concentration is very critical, but it can be controlled precisely. Aluminum must be removed continuously from the new techology cells. Concepts to accomplish it have been formulated, but R&D funding is required to reduce them to practice.

Table 3
Major Tradeoffs for Proposed New Technology
Compared to Existing Technology

POSITIVE TRADEOFFS	HALL-HEROULT	NON-CONSUMABLE ANODE/SLURRY
Size of Cells and Plant Capital Cost	Large	Considerable Decrease
Specific Energy Consumption kWh/Kg	13-17	11
Carbon Anode Production	Essential	Eliminate
Labor to Change Anodes	Essential	Eliminate
CO_2 and CF Compounds	May be CO_2 and PFC Tax	Eliminate
Ledges, Crust, and Muck	Big Problem to Control	Eliminate
Bath Temperature Measurement	Intermittent Infrequent	Continuous and Inexpensive
Potroom Fume Collection and Treatment	Big System	Smaller System with less air leakage at cell
NEGATIVE TRADEOFFS		
Alumina Particle Size	Standard Reduction Grade	May Need Finer or More-Friable Particles
Metal Removal from Cell	Daily	Continuous; New Technology Being Developed

ACKNOWLEDGMENT

The author acknowledges the contributions of Richard J. Brooks of Brooks Rand, Ltd., who collaborated on the process development, and of Prof. Jomar Thonstad of the Institute of Technical Electrochemistry in Trondheim who consulted on the scientific aspects. The work was supported by National Science Foundation SBIR Phase I and II Grants and a U.S. Department of Energy, Energy Related Inventions Program Grant.

REFERENCES

1. K. Billehaug and H.A. Øye, "Inert Cathodes for Aluminum Electrolysis in Hall-Heroult Cells," Aluminium, 56 (1980), 642-648 and 713-718.

2. K. Billehaug and H.A. Øye, "Inert Cathodes for Aluminum Electrolysis in Hall-Heroult Cells," Aluminium, 57 (1981), 146-150 and 228-231.

3. T.R. Beck, J.C. Withers, and R.O. Loutfy, "Composite-Anode Aluminum Reduction Technology," Light Metals 1986, (Warrendale, PA, TMS-AIME, 1986), 261-266.

4. Alcoa Final Report, "Inert Anodes for Aluminum Smelting," DOE Contract DOE/CS/40158-20, February, 1986.

5. W.C. Sleppy and C.N. Cochran, "Bench Scale Electrolysis of Alumina in Sodium Fluoride-Aluminum Fluoride melts below 900°C," Light Metals 1979, p 385, The Metallurgical Society, Warrendale, PA 1979.

6. R. Piontelli, B. Mazza, and P. Pedeferri, "Anodic and Cathodic Behavior of Melted Aluminum Electrodes in Cryolyte Baths," Electrochim. Metallorum, 1 (2) 217 (1966).

7. K. Grjotheim, C. Crohn, M. Malinovsky, K. Matiasovsky, and J. Thonstad, "Aluminium Electrolysis," 2nd Ed., Aluminum-Verlag, Dusseldorf, 1982.

8. E.M. Lewis, C.R. Robbins, and H.F. McMurdic, "Phase Diagrams for Ceramists," Ed., M.K. Reser, Nat. Bur. Standards and Am. Ceram. Soc., Ohio, 1969.

9. R.H. Perry, "Chemical Engineers Handbook," 5th Ed., McGraw Hill, New York, 1979.

10. R.B. MacMullin, "The Problem of Scale-Up in Electrolytic Processes," Electrochemical Technology, 1, 5 (1963).

11. J. Thonstad, personal communication, data presented in Trondheim Aluminum Course.

12. JANAF Thermochemical Tables, 2nd Ed., Nat. Bur. Stand., NSRDS-NBS37, 1971.

13. R.E. Meredith and C.W. Tobias, "Conduction in Heterogeneous Systems," in Advances in Electrochemistry and Electrochemical Engineering, 2, (1962), P. Delahay and C.W. Tobias, Eds., John Wiley, NY 15-47.

14. T.R. Beck and R.J. Brooks, "Method and Apparatus for Electrolytic Reduction of Alumina," U.S. Patent No. 4,592,812, 1986.

15. T.R. Beck and R.J. Brooks, "Electrolytic Reduction of Alumina," U.S. Patent No. 4,865,701, 1989.

16. T.R. Beck and R.J. Brooks, "Electrolytic Reduction of Alumina," U.S. Patent No. 5,006,209, 1991.

17. T.R. Beck, I. Rousar, and J. Thonstad, "Energy Efficiency Considerations on Monopolar versus Bipolar Fused Salt Elecctrolysis Cells," Light Metals 1993 (Warrendale, PA, TMS-AIME).

18. R.D. Waldron, "Alternatives for In Situ Resource Processing," in Engineering, Construction and Operations in Space II, Proceedings of Space 90, Ed., S.W. Johnson and J.P. Wetzel, ASCE, New York, 1990.

19. D. Morton, "Today's Aluminum Industry: Facing the Economic and Environmental Challenges," J. Metals, 44, 6 (1992).

20. P. Zorer, "Perfluorocarbons Use Emissions May Face Restriction," Chem. & Eng. News, Aug 9 (1993), 16.

NOMENCLATURE

a = a constant
A = area, cm^2
C = concentration, mol/cm^3
D = diffusion coefficient, cm^2/s
F = Faraday, 95,600 A·s/eq
g = gravitational constant, 980 cm/s^2
i = current density, A/cm^2
I = current, A
j = flux, $mol/cm^2 \cdot s$
k = mass transfer coefficient, cm/s
K = 3 $Fk\Delta C$, A/cm^2
ℓ = anode-cathode spacing, cm
r = particle radius, cm
R = rate, mol/s
t = time, min
W = weight percent of Al_2O_3
x = distance, cm
y = mol% AlF_3
u_t = terminal velocity, cm/s
δ_N = Nernst diffusion layer thickness, cm
ϵ = current efficiency, dimensionless
κ = electrical conductivity, S/cm
ρ = density, g/cm^3
μ = viscosity, g/s·cm

Subscripts

a = anode	s = saturation
b = bulk or bath	t = terminal or total
e = electrolyte	x = position
L = limiting	
N = Nernst	
P = particle or parasitic	